Generation and Characterization of the $C_3O_2^-$ Anion with an Unexpected Unsymmetrical Structure

Lina Wang+, Sudip Pan+, Bo Lu, Xuelin Dong, Hongmin Li, Guohai Deng, Xiaoqing Zeng, Mingfei Zhou,* and Gernot Frenking*

***Abstract:** The carbon suboxide anion $C_3O_2^-$ is generated in solid neon matrix. It is characterized by infrared absorption spectroscopy as well as quantum chemical calculations to have a planar C_s structure where two CO groups with significantly different bond lengths and angles are attached in a zigzag fashion to the central carbon atom. Bonding analysis indicates that it is best described by the bonding interactions between a neutral CO in a triplet excited state and a doublet excited state of CCO^-.*

Carbon suboxide with a chemical formula C_3O_2 is a long known stable dioxide of carbon.[1] Early spectroscopic and electron diffraction investigations suggest that the molecule has a symmetrical linear structure.[2,3] The bonding was conventionally described in common textbooks as linear cumulene valence structure O=C=C=C=O involving four double bonds.[4] Later high resolution infrared spectroscopic investigations indicate that the molecule is bent with an angle of 156° at the central carbon atom in the gas phase.[5] This is in excellent agreement with high level ab initio calculations at the CCSD(T)/cc-pVQZ level, which predicted a bond angle of 155.9°.[6] The bending potential is very flat (< 0.5 kcal mol^{-1}), and the molecule becomes linear in the solid state.[7] The deviation from linearity and the very shallow bending potential of carbon suboxide are difficult to explain with the

standard electron-sharing bonding model of a cumulene, while it becomes plausible when the donor-acceptor model is employed.[8] The ground-state of bent C_3O_2 molecule can be classified as a dicarbonyl complex of carbon in its ^1D excited state with an electron configuration $(2s)^0$ $(2p_\sigma)^2$ $(2p_{\pi\parallel})^0$ $(2p_{\pi\perp})^2$.[9] Thus, C_3O_2 is a divalent carbon (0) complex termed as carbones.[10]

The positively charged $C_3O_2^+$ complex has also been generated in the gas phase, which was characterized to have a bent C_{2v} structure with a more acute bending angle than in neutral C_3O_2.[11] The smaller bending angle of the cation relative to the neutral comes from the weaker $OC \leftarrow C \rightarrow CO$ π-back donation interaction than that in the neutral complex. In view of this, one would expect that the negatively charged $C_3O_2^-$ anion should have linear or near linear structure. Previous thermal electron attachment experiment in the gas phase showed that C_3O_2 can capture thermal electrons,[12] but the formation of a stable negative ion is not achieved in the form of $C_3O_2^-$ as C_3O_2 was predicted to have a negative electron affinity.[13] The negative ions were suggested to be stabilized in the form of a dimer or other complex negative ions.[12] It is known that the anions of species with a negative electron affinity such as CO_2^- can be trapped and stabilized in low temperature solid noble gas matrices.[14] Here we show that the isolated carbon suboxide anion $C_3O_2^-$ can be prepared in solid neon matrix. Infrared spectroscopy in conjunction with state-of-the-art quantum chemical calculations confirm that the anion has an unexpected non-linear structure where two CO groups with significantly different bond lengths and angles are attached in a zigzag fashion to the central carbon atom, which can be regarded as bonding between a neutral CO fragment in a triplet excited state and a doublet excited state of CCO^- fragment.

The $C_3O_2^-$ anion was produced by concurrent codeposition of pulsed laser-ablated metal atoms and electrons with C_3O_2/Ne mixtures at 4 K as described in detail previously.[15] The product species are detected by infrared absorption spectroscopy employing a Bruker Vertex 80 V spectrometer at 0.5 cm^{-1} resolution using a liquid-nitrogen cooled mercury cadmium telluride (MCT) detector. Carbon suboxide was prepared by heating a mixture of malonic acid and excessive P_2O_5 at 140°C in a glass vessel that is connected to the dynamic vacuum line.[2a] The sample was purified via several freeze-pump-thaw cycles before use. Experiments were performed using over 10 different metal targets. A group of product absorptions at 2075.7, 1738.1, 1403.0 and 811.5 cm^{-1} are observed after sample deposition at 4 K, which get decreased together upon red light (625 nm) irradiation, and almost disappear under blue light (440 ± 20 nm) irradiation.

[*] L. Wang,[+] B. Lu, X. Dong, H. Li, G. Deng, X. Zeng, M. Zhou
Collaborative Innovation Center of Chemistry for Energy Materials, Department of Chemistry, Shanghai Key Laboratory of Molecular Catalysts and Innovative Materials, Fudan University
Shanghai 200438 (China)
E-mail: mfzhou@fudan.edu.cn

S. Pan,[+] G. Frenking
Institute of Advanced Synthesis, School of Chemistry and Molecular Engineering, Jiangsu National Synergetic Innovation Center for Advanced Materials, Nanjing Tech University
Nanjing 211816 (China)
and
Fachbereich Chemie, Philipps-Universität Marburg
Hans-Meerwein-Strasse 4, 35043 Marburg (Germany)
E-mail: frenking@chemie.uni-marburg.de

[+] These authors contributed equally to this work.

Supporting information and the ORCID identification number(s) for the author(s) of this article can be found under:
https://doi.org/10.1002/anie.202013921.

Their intensity cannot be recovered on subsequent sample annealing to high temperatures. The difference spectrum shown in Figure 1 clearly demonstrates that along with the elimination of this group of product absorptions, the absorptions of neutral C_3O_2 increase in concert. This group of product absorptions is observed in all the experiments with different metal targets, indicating that the absorber is metal independent and is due to a reaction product involving the common reagent, namely the electrons produced in the pulsed laser ablation process. All the four absorptions are red-shifted when a $^{13}C(^{12}CO)_2$ sample is used (See Table 1). The experiment with equal molar mixture of C_3O_2 and $^{13}C(^{12}CO)_2$ confirms that only one C_3O_2 unit is involved in the absorber (Figures S1 and S2). An additional experiment was performed by adding CCl_4 to serve as an electron trap to verify that the observed species is an anion.[16] As shown in Figure S3, this group of product absorptions is almost absent from the spectrum with 0.025 % CCl_4 added to the neon matrix gas. These experimental observations indicate that the observed absorptions can clearly be assigned to the $C_3O_2^-$ anion.

We calculated the equilibrium geometry and the vibrational spectrum of the $C_3O_2^-$ anion at the CCSD(T)-Full/

def2-TZVPPD level of theory in order to verify the experimental assignment. Figure 2 shows the computed geometry, and the bond lengths and angles. The $C_3O_2^-$ anion has a planar but otherwise highly asymmetric structure where two CO groups with significantly different bond lengths and angles are attached in a zigzag fashion to the central carbon atom with a bending angle of 144.4°. One CO group has a rather short C-CO bond length of 1.274 Å, which is even shorter than in neutral $C(CO)_2$ (1.284 Å)[6] whereas the other CO group has a much longer C-CO bond with an interatomic distance of 1.381 Å. The latter carbonyl ligand has a bending angle of 137.1° and a longer C-O distance of 1.217 Å whereas the former CO group is nearly linearly bonded with a bending angle of 172.8° and a C−O bond length of 1.206 Å. The electronic ground state of the $C_3O_2^-$ anion is $^2A'$. The molecule is thermodynamically stable at 298 K for loss of one CO by $\Delta G^{298} = 30.8$ kcal mol^{-1}. The total binding energy of two CO ligands is $\Delta G^{298} = 100.6$ kcal mol^{-1}. Table 1 shows also the calculated vibrational frequencies and isotopic frequency shifts of the four observed vibrations of $C_3O_2^-$. The calculated wavenumbers of the harmonic vibrations are as usual slightly higher than the experimental inharmonic modes. The otherwise excellent agreement between the experimental and calculated vibrational frequencies and particularly the frequency shifts of the $^{13}C(^{12}CO)_2^-$ isomer leave no doubt that the observed species is the $C_3O_2^-$ anion in the $^2A'$ electronic ground state.

We analysed the electronic structure and bonding situation of the $C_3O_2^-$ anion with various charge- and energy decomposition methods. Figure 2 gives also the atomic partial charges using the NBO 6.0 method.[17] The central divalent carbon atom carries a large negative charge of -0.75 e, which is the same as for the much more electronegative oxygen atoms. The spin density distribution of the unpaired electrons is also
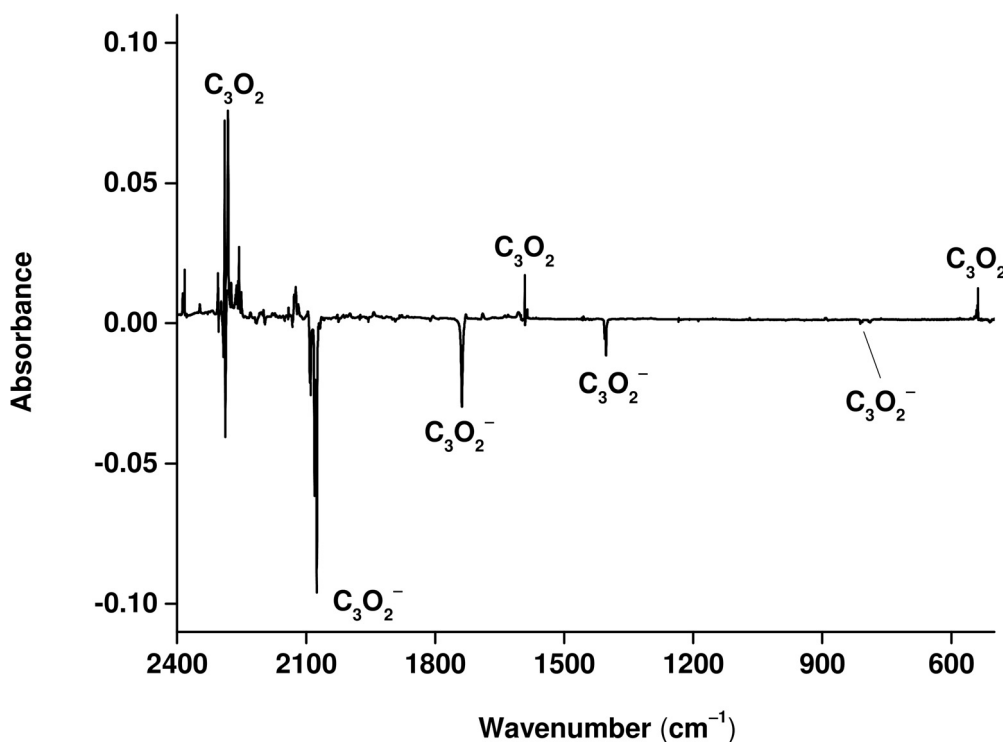

Figure 1. IR difference spectrum in the 2400–500 cm^{-1} region from co-deposition of laser-ablated boron atoms and electrons with 0.05 % C_3O_2 in neon. Spectrum taken after 10 min of blue light irradiation minus the spectrum taken after 30 min of sample deposition at 4 K.

Table 1: Experimentally observed (in Ne) and calculated vibrational frequencies and the isotopic frequency shifts Δ (cm^{-1}) of $C_3O_2^-$.

	Exptl.			Calcd.	
$^{12}C_3O_2^-$	$^{13}C(^{12}CO)_2^-$	Δ	$^{12}C_3O_2^-$	$^{13}C(^{12}CO)_2^-$	Δ
2075.7	2058.3	−17.4	2126.2	2106.2	−20.0
1738.1	1732.6	−5.5	1761.1	1755.8	−5.3
1403.0	1376.7	−26.3	1429.1	1402.0	−27.1
811.5	806.5	−5.0	842.3	835.8	−6.5

$C_3O_2^- \rightarrow C^- (^4S) + 2CO; D_0 (\Delta G^{298}) = 116.3 (100.6)$

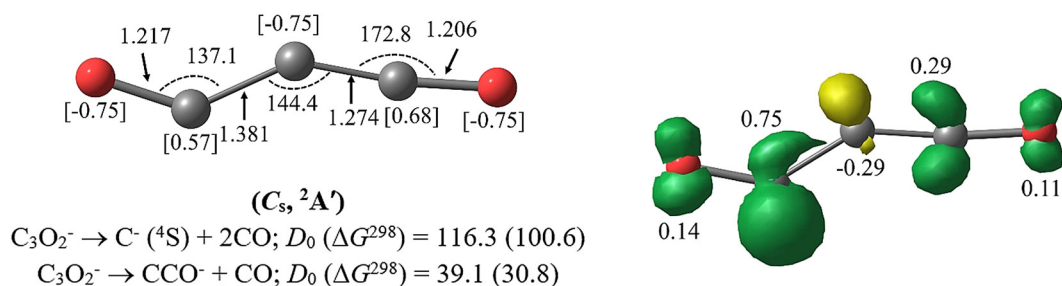$C_3O_2^- \rightarrow CCO^- + CO; D_0 (\Delta G^{298}) = 39.1 (30.8)$

Figure 2. Calculated equilibrium geometry (left) and spin density distribution (right) of $C_3O_2^-$ at the CCSD(T)-Full/def2-TZVPPD level. Bond lengths are in [Å] and bond angles are in [°]. The bond dissociation energies are in kcal mol^{-1}. The partial natural charges on each atomic centre are given in square brackets. The value of natural spin density on each atomic centre is given in e unit. The isovalue is 0.02 au.

shown in Figure 2. It is apparent that the CO group, which has a longer C-CO bond, carries most of the spin density. Since the energetically most accessible dissociation pathway is the loss of one CO group (Figure 2), we envisaged the $C_3O_2^-$ anion as the product of CO addition to the CCO$^-$ anion. Calculations using the EDA (Energy decomposition analysis)[18] method in conjunction with the NOCV (Natural Orbitals for Chemical Valence)[19] approach are performed. The results using the fragments CCO$^-$ and the distant CO group in different electronic states as interacting moieties are given in Table S1 of Supporting Information. The results

showed that the bonding situation is best described using CO in the $^3\Pi$ excited triplet state and the CCO$^-$ anion in the excited $^2\Sigma$ state. This comes from the lowest orbital relaxation energy ΔE_{orb} of the EDA-NOCV[20] calculations when the triplet state of CO and the excited $^2\Sigma$ state of CCO$^-$ rather than the other electronic states are employed, which has been proven as useful measure for finding the best fragments for the orbital interactions.[21] Figure 3 shows the orbital correlation diagram for the orbital interactions between triplet ($^3\Pi$) CO and doublet ($^2\Sigma$) CCO$^-$. The unpaired electrons in the σ MOs of CO (5σ) and CCO$^-$ (7σ) form a strong electron-
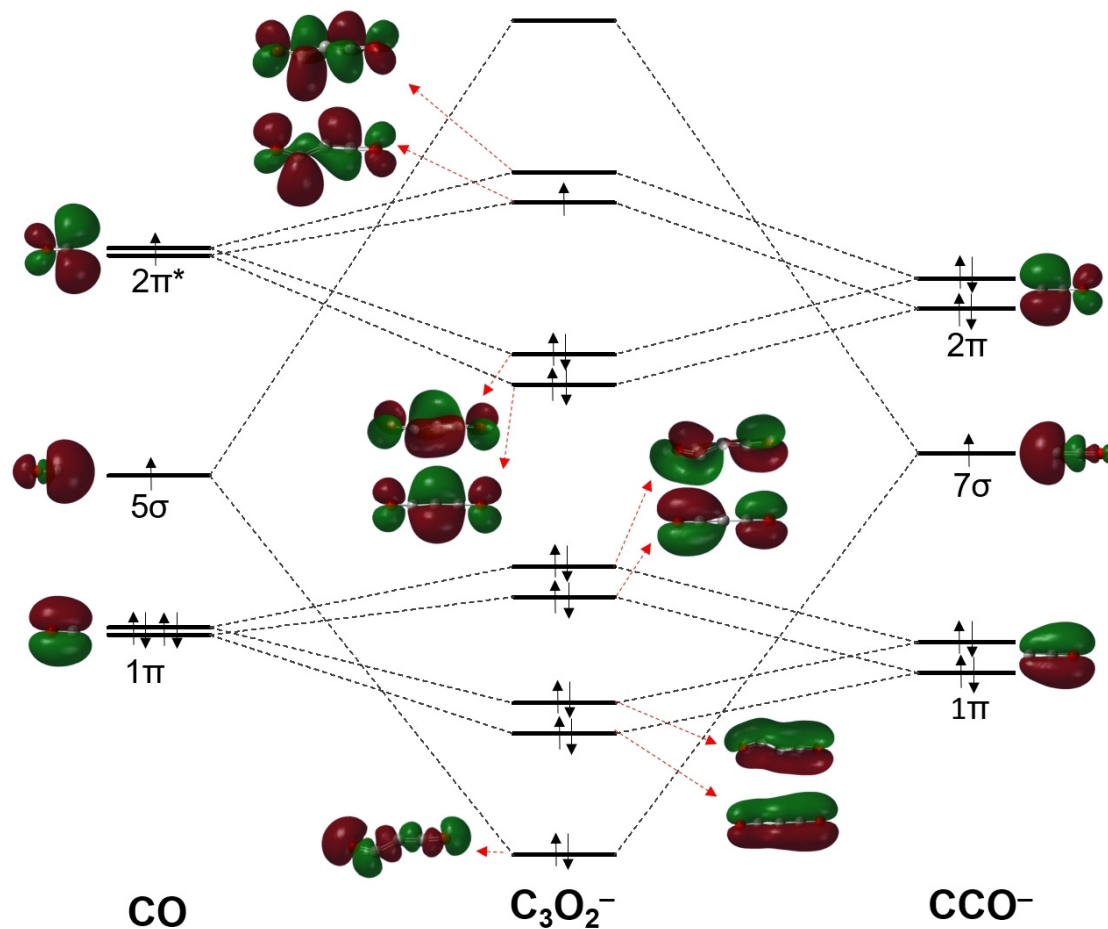

Figure 3. The bonding scheme of the $C_3O_2^-$ anion, qualitatively illustrating the bonding interactions between CO and CCO$^-$. The canonical Kohn–Sham frontier valence MOs of CO, CCO$^-$ and $C_3O_2^-$ are plotted with isosurfaces = 0.03 au.

sharing bond whereas the unpaired electron in the 2π MO of CO interacts with the electrons in the fully occupied 2π MOs of CCO$^-$. But the two fragments approach each other in a non-linear fashion, which makes it possible that the in-plane σ and π MOs mix. The unpaired electron in the 2π MO of CO can also couple with the unpaired electron of CCO$^-$. A more detailed and quantitative analysis of the orbital interactions is provided by EDA-NOCV calculations.

Table 2 shows the numerical EDA-NOCV results of C$_3$O$_2^-$ using CCO$^-$ in the $^2\Sigma$ doublet state and the more distant CO ($^3\Pi$) ligand as interacting fragments. The results show that the attractive interactions have a slightly more covalent character ($\Delta E_{orb} = 59\%$) than electrostatic origin ($\Delta E_{elstat} = 41\%$). The breakdown of ΔE_{orb} in pairwise orbital interactions suggests that the dominant contribution $\Delta E_{orb(1)}$ comes from the electron-sharing interaction between the unpaired electrons of ($^3\Pi$) CO and the unpaired electron of ($^2\Sigma$) CCO$^-$, which provides 69% of the covalent bonding. This

becomes obvious by inspecting the associated deformation density $\Delta\rho_{(1)}$ and the connected fragment orbitals, which are displayed in Figure 4. The second strongest orbital term
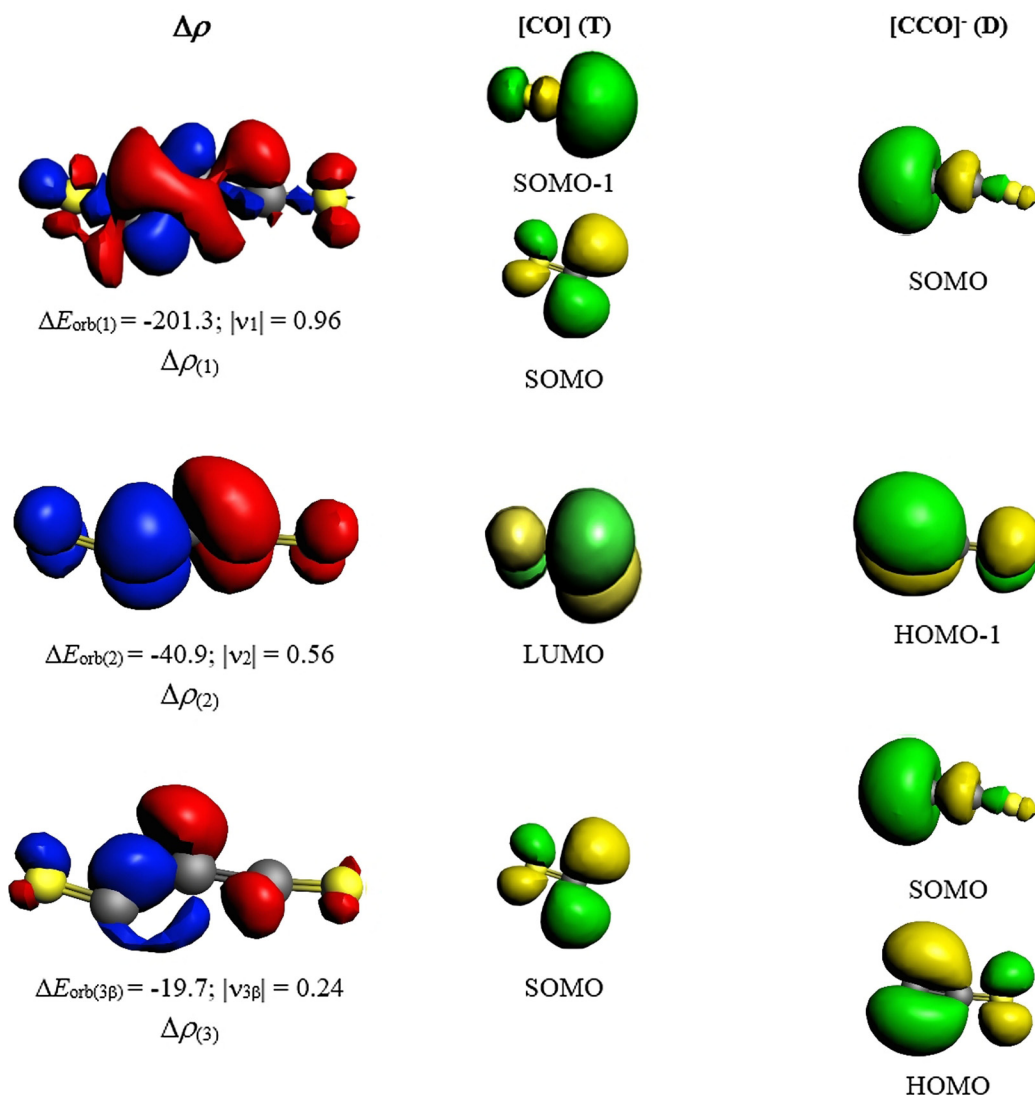

Figure 4. Plot of the deformation densities $\Delta\rho$ and the connected most important fragment orbitals at the M06-2X/TZ2P//CCSD(T)-Full/def2-TZVPPD level, which are associated to the orbital interactions $\Delta E_{orb(1)} - \Delta E_{orb(3)}$ in C$_3$O$_2^-$ between the fragments ($^3\Pi$) CO and ($^2\Sigma$) CCO$^-$ as interacting moieties (Table 2). The orbital energy values are given in kcal mol^{-1}. The charge flow of the deformation densities is red→blue. The isosurface value is 0.001 au. Charge eigenvalues $|\nu|$ show the total electron movement.

Table 2: EDA-NOCV results at the M06-2X/TZ2P//CCSD(T)-Full/def2-TZVPPD level of C$_3$O$_2^-$ using the fragments ($^3\Pi$) CO and ($^2\Sigma$) CCO$^-$ as interacting moieties. Energy values are given in kcal mol^{-1}.

Energy	Orbital Interaction	($^3\Pi$) CO + ($^2\Sigma$) CCO$^-$
ΔE_{int}		−230.7
ΔE_{Pauli}		258.6
$\Delta E_{Metahybrid}$		6.1
ΔE_{elstat} [a]		−204.1 (41.2%)
ΔE_{orb} [a]		−291.3 (58.8%)
$\Delta E_{orb(1)}$ [b]	[OC]-[CCO]$^-$ electron-sharing σ bond	−201.3 (69.1%)
$\Delta E_{orb(2)}$ [b]	[OC]←[CCO]$^-$ π-backdonation	−40.9 (14.0%)
$\Delta E_{orb(3)}$ [b]	Polarization and [OC]←[CCO]$^-$ σ bonding	−19.7 (6.8%)
$\Delta E_{orb(rest)}$ [b]		−29.4 (10.2%)

[a] The values in parentheses give the percentage contribution to the total attractive interactions $\Delta E_{elstat} + \Delta E_{orb}$. [b] The values in parentheses give the percentage contribution to the total orbital interactions ΔE_{orb}.

$\Delta E_{orb(2)}$ comes from the $[OC] \leftarrow [CCO]^-$ π backdonation whereas $\Delta E_{orb(3)}$ is due to a mixing of the 2π HOMO and the 7σ SOMO of CCO$^-$ and coupling with the 2π* SOMO of CO. The remaining stabilizing orbital interactions come mainly from the polarization of the fragments. We want to point out that the deformation densities $\Delta \rho_{(1)}$ and $\Delta \rho_{(2)}$ shown in Figure 4 come from adding the deformation densities of the α and β electrons, which opposite directions. The individual one-electron components of $\Delta \rho_{(1)}$ and $\Delta \rho_{(2)}$ are shown in Figure S5 of Supporting Information. The electron flows of the α and β electrons explain the negative value of the spin density at the central carbon atom of the $C_3O_2^-$ anion.

The information about the bonding situation in the $C_3O_2^-$ anion gained by the EDA-NOCV analysis may be expressed in the Lewis type picture shown in Figure 5, which qualitatively depicts the nature of the interatomic interaction. There is an electron-sharing σ bond and a one electron dative π bond between the [CCO] moiety and the left CO group, which has three lone-pairs at oxygen and one lone-pair at the carbon atom. There are further mesomeric forms, which can be depicted for the $C_3O_2^-$ anion. But one must be aware that the very useful Lewis structures are only a qualitative and rather crude description of the actual electronic structure of a molecule. Chemical binding theory has evolved greatly in recent decades, and methods such as EDA-NOCV are now available to provide more detailed information about the nature of interatomic interactions.
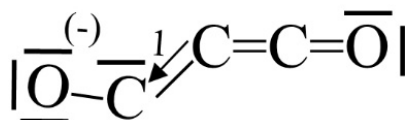

Figure 5. Sketch of a possible Lewis structure of the $C_3O_2^-$ anion.

We have also calculated the geometries and bond dissociation energies (BDEs) of the isoelectronic species $N(CO)_2$ and $O(CO)_2^+$, which have not been observed so far. Figure S4 of Supporting Information shows that both molecules have a similar C_s equilibrium geometry and a $^2A'$ electronic ground state. The difference between the bond lengths of the two CO ligands to the central atom in the $E^q(CO)_2$ molecules increases with the order of $C^- < N < O^+$. The calculated BDE for CO loss indicates that $N(CO)_2$ ($\Delta G^{298} = 13.5$ kcal mol^{-1}) and $O(CO)_2^+$ ($\Delta G^{298} = 21.0$ kcal mol^{-1}) may be observable under appropriate experimental conditions.

In summary, we report the generation and spectroscopic characterization of the $C_3O_2^-$ anion, which according to quantum chemical calculations has a planar C_s symmetry where two CO groups with significantly different bond lengths and angles are attached in a zigzag fashion to the central carbon atom. Bonding analysis indicates that it is best described by the bonding interactions between a neutral CO in a triplet excited state and a doublet excited state of CCO$^-$, in contrast to the neutral and cation, both of which have symmetric structures that can be classified as dicarbonyl complexes of carbon atom or cation.

[1] O. Diels, B. Wolf, *Ber. Dtsch. Chem. Ges.* **1906**, *39*, 689–697.
[2] a) D. A. Long, F. S. Murfin, R. L. Williams, *Proc. R. Soc. London Ser. A* **1954**, *223*, 251–266; b) H. D. Rix, *J. Chem. Phys.* **1954**, *22*, 429–433; c) F. A. Miller, W. G. Fateley, *Spectrochim. Acta* **1964**, *20*, 253–266; d) L. A. Carreira, R. O. Carter, J. R. Durig, R. C. Lord, C. C. Milionis, *J. Chem. Phys.* **1973**, *59*, 1028–1037; e) P. R. Bunker, B. M. Landsberg, *J. Mol. Spectrosc.* **1977**, *67*, 374–385; f) P. R. Bunker, *J. Mol. Spectrosc.* **1980**, *80*, 422–437.
[3] M. Tanimoto, K. Kuchitsu, Y. Morino, *Bull. Chem. Soc. Jpn.* **1970**, *43*, 2776–2785.
[4] a) L. H. Reyerson, K. Kobe, *Chem. Rev.* **1930**, *7*, 479–492; b) R. L. Livingston, C. N. R. Rao, *J. Am. Chem. Soc.* **1959**, *81*, 285–287; c) P. Pyykkö, N. Runeberg, *J. Mol. Struct. THEOCHEM* **1991**, *234*, 279–290.
[5] a) P. Jensen, J. W. C. Johns, *J. Mol. Spectrosc.* **1986**, *118*, 248–266; b) J. Vander Auwera, J. W. C. Johns, O. L. Polansky, *J. Chem. Phys.* **1991**, *95*, 2299–2316.
[6] J. Koput, *Chem. Phys. Lett.* **2000**, *320*, 237–244.
[7] A. Ellern, T. Drews, K. Seppelt, *Z. Anorg. Allg. Chem.* **2001**, *627*, 73–76.
[8] M. A. Celik, R. Sure, S. Klein, R. Kinjo, G. Bertrand, G. Frenking, *Chem. Eur. J.* **2012**, *18*, 5676–5692.
[9] G. Frenking, *Angew. Chem. Int. Ed.* **2014**, *53*, 6040–6046; *Angew. Chem.* **2014**, *126*, 6152–6158.
[10] R. Tonner, G. Frenking, *Chem. Eur. J.* **2008**, *14*, 3260–3272.
[11] J. Y. Jin, L. L. Zhao, X. N. Wu, W. Li, Y. H. Liu, D. M. Andrada, M. F. Zhou, G. Frenking, *J. Phys. Chem. A* **2017**, *121*, 2903–2910.
[12] H. Shimamori, E. Suzuki, Y. Hatano, H. Nonaka, Y. Ohshima, T. Kondow, K. Kuchitsu, *J. Chem. Phys.* **1989**, *91*, 4148–4154.
[13] H. Nonaka, M. Uematsu, K. Yamanouchi, T. Kondow, K. Kuchitsu, *Chem. Phys.* **1989**, *133*, 165–171.
[14] a) W. E. Thompson, M. E. Jacox, *J. Chem. Phys.* **1999**, *111*, 4487–4496; b) M. F. Zhou, L. Andrews, *J. Chem. Phys.* **1999**, *110*, 2414–2422.
[15] G. J. Wang, M. F. Zhou, *Int. Rev. Phys. Chem.* **2008**, *27*, 1–25.
[16] M. F. Zhou, L. Andrews, *J. Am. Chem. Soc.* **1998**, *120*, 11499–11503.
[17] E. D. Glendening, C. R. Landis, F. Weinhold, *J. Comput. Chem.* **2013**, *34*, 1429–1437.
[18] T. Ziegler, A. Rauk, *Theor. Chim. Acta* **1977**, *46*, 1–10.
[19] a) M. Mitoraj, A. Michalak, *J. Mol. Model.* **2007**, *13*, 347–355; b) M. Mitoraj, A. Michalak, *Organometallics* **2007**, *26*, 6576–6580.

[20] a) A. Michalak, M. Mitoraj, T. Ziegler, *J. Phys. Chem. A* **2008**, *112*, 1933–1939; b) M. P. Mitoraj, A. Michalak, T. Ziegler, *J. Chem. Theory Comput.* **2009**, *5*, 962–975.

[21] a) Q. Zhang, W.-L. Li, C. Xu, M. Chen, M. Zhou, J. Li, D. M. Andrada, G. Frenking, *Angew. Chem. Int. Ed.* **2015**, *54*, 11078–11083; *Angew. Chem.* **2015**, *127*, 11230–11235; b) D. M. Andrada, G. Frenking, *Angew. Chem. Int. Ed.* **2015**, *54*, 12319–12324; *Angew. Chem.* **2015**, *127*, 12494–12500; c) C. Mohapatra, S. Kundu, A. N. Paesch, R. Herbst-Irmer, D. Stalke, D. M. Andrada, G. Frenking, H. W. Roesky, *J. Am. Chem. Soc.* **2016**, *138*, 10429–10432; d) L. T. Scharf, M. Andrada, G. Frenking, V. H. Gessner, *Chem. Eur. J.* **2017**, *23*, 4422–4434; e) M. Hermann, G. Frenking, *Chem. Eur. J.* **2017**, *23*, 3347–3356; f) D. C. Georgiou, L. Zhao, D. J. D. Wilson, G. Frenking, J. L. Dutton, *Chem. Eur. J.* **2017**, *23*, 2926–2934; g) Z. Wu, J. Xu, L. Sokolenko, Y. L. Yagupolskii, R. Feng, Q. Liu, Y. Lu, L. Zhao, I. Fernández, G. Frenking, T. Trabelsi, J. S. Francisco, X. Zeng, *Chem. Eur. J.* **2017**, *23*, 16566–16573; h) D. M. Andrada, J. L. Casalz-Sainz, A. M. Pendás, G. Frenking, *Chem. Eur. J.* **2018**, *24*, 9083–9089; i) R. Saha, S. Pan, G. Merino, P. K. Chattaraj, *Angew. Chem. Int. Ed.* **2019**, *58*, 8372–8377; *Angew. Chem.* **2019**, *131*, 8460–8465; j) Q. Wang, S. Pan, Y. Wu, G. Deng, J.-H. Bian, G. Wang, L. Zhao, M. Zhou, G. Frenking, *Angew. Chem. Int. Ed.* **2019**, *58*, 17365–17374; *Angew. Chem.* **2019**, *131*, 17526–17535.